Available online at www.sciencedirect.com
ScienceDirect
Journal of Sound and Vibration 303 (2007) 691–706
JOURNAL OF SOUND AND VIBRATION
www.elsevier.com/locate/jsvi

Closed-form solutions for the structural response to train loads

F. Vestroni*, S. Vidoli

Dipartimento di Ingegneria Strutturale e Geotecnica, Università di Roma "La Sapienza", Via Eudossiana 18, 00184 Rome, Italy

Received 9 February 2005; received in revised form 8 January 2007; accepted 24 January 2007
Available online 12 April 2007

Abstract

Exact analytic solutions for uniform, equally spaced sequences of travelling point loads, loading a continuous finite-length structure, are found. A general procedure to reduce any train to this kind of sequence, whilst preserving the essential features of its dynamic load, is also introduced. The analytic expressions provided make it possible to derive the main choices for both structural designs and monitoring tests. A comparison between analytic predictions and numerical results for a case study is presented and discussed.

1. Introduction

There are several reasons for the increasing interest of the engineering community in the subject of dynamic loads induced by train traffic [1]. The increasing speeds of trains produce high levels of structural vibrations [2]; thus the design of structures to support railways requires accurate knowledge of traffic loads. Moreover, health monitoring tests on bridges and railroads are often based on comparison of structural responses to assigned train passages [3]. To design and process these tests efficiently, a deep understanding of the dynamic characteristics of traffic loads is needed. Whereas vehicular traffic induces mainly random loads [4], the dynamic load associated with the passage of a train is characterized by a set of frequency peaks [5].

Several kinds of structure supporting the train passages have been examined in the literature: beam-like structures [6,7], bridges [8,9], discrete supports [10], layered grounds [11]. Some closed-form solutions are found in Ref. [12], where a time-domain approach is used to analyze the structural response to train passages. In this paper, advantage is taken of a frequency-domain approach to find simple closed-form relationships among the relevant parameters of the problem; the characteristic frequencies of train loads are analytically expressed as functions of the main descriptors of the convoy (interaxle distances, weights, speed). The aim is to derive both structural design and health monitoring choices with manageable expressions of the solutions.

Some refined models of dynamic train–bridge interactions have already been developed, see for instance Refs. [13–15]; typically, the frequency range in which these interactions can be neglected goes from 0 up to 50 Hz for standard railway bridges. Hence, since a relevant number of structural modes occurs within this frequency interval, the interactions between the train and the underlying structure is here neglected and the

*Corresponding author: Tel.: +39 6 44585198; fax: +39 6 4884852.
E-mail address: vestroni@uniroma1.it (F. Vestroni).

0022-460X/$ - see front matter
doi:10.1016/j.jsv.2007.01.040

vertical train loads are modelled as a sequence of moving point loads. We refer to the appendix for a more careful analysis of this assumption. A general procedure is then discussed to transform any train to one uniform and equally spaced sequence of impulses, while preserving the main features of its dynamic load. Using this simplifying hypothesis an exact and manageable analytical solution is found for the phase and modulus of the Fourier transform (FT) of the load, enlightening important aspects of the dynamic train load. Furthermore, the projection of the load on the spatial modes of the supporting structure makes it possible to calculate some bounds of the structural response and to predict, in general, the values of the train parameters (velocity, characteristic wagon length, number of wagons) leading to critical structural conditions. The analytical solution considered is successfully compared with numerical results for the case of a high-speed ETR500 train travelling over a one-span arched bridge.

2. Travelling sequences of point loads

When the elastic interaction between the vertical dynamics of the wagons and the underlying structure is neglected, only the weight and centrifugal accelerations of the train contribute to the applied load. The time-varying inertia of the train has also been neglected, its effects on the structural dynamics being bounded by the ratio between the train and bridge masses (often this ratio does not exceed 5%). A discussion of the limits of this assumption is reported in Appendix A, while a comparison of the available numerical methods for the analysis of vehicle–structure interactions can be found in Ref. [16].

The track is here thought of as a smooth planar curve $\mathscr{C}$ with curvilinear abscissa x. The in-plane vector field everywhere normal to $\mathscr{C}$ is labelled as $\mathbf{n}(x)$ while $\mathbf{e}$ represents the out-of-plane unit vector. The train is thought of as a travelling sequence of point loads centered in the current positions of its wheels; the intensity of each impulse is determined by the static weight acting on each wheel, while the centrifugal force is assumed to be proportional to the static weight. To represent the point loads, the Dirac delta functions are used, allowing for exact analytic treatment. As a constant velocity v_T is considered for the train, the force acting on the track $\mathscr{C}$ at time t is given by

$$f(x,t)=\sum_{j=1}^{J}[W_j\mathbf{e}+C_j\mathbf{n}(x)]\delta(x_{0j}+v_Tt-x),\quad x\in\mathscr{C}, \tag{1}$$

where x_{0j} denotes the initial ($t=0$) position of the jth wheel, W_j and C_j, respectively, represent the weight and the centrifugal force acting on the jth wheel. The summation is extended to the total number J of train wheels. This explicit and simple dependence of the load $f(x,t)$ on the time variable t allows for an exact evaluation of its FT. The case of a non-constant velocity, i.e. a decelerating or accelerating train, where forces tangent to the track are induced, will not be considered here. For a constant train speed, the centrifugal loads $C_j\equiv v_T^2W_j/(gR)$ are proportional to the static weights assigned to each wheel, with R and g being the radius of curvature of the track and the acceleration of gravity, respectively.

Once the following dimensionless quantities have been defined:

$$s=\frac{x}{L_w},\quad \tau=\varpi t,\quad \upsilon=\frac{v_T}{\varpi L_w},\quad \Delta_j=\frac{W_j}{\varpi^2ML_w}, \tag{2}$$

the dimensionless expression of the load (1) on the track reads:

$$\hat{f}(s,\tau)=\left(\mathbf{e}+\frac{v_T^2}{Rg}\,\mathbf{n}(s)\right)p(s,\tau),$$
$$p(s,\tau)\coloneqq\sum_{j=1}^{J}\Delta_j\delta(s_{0j}+\upsilon\tau-s). \tag{3}$$

Here L_w, ϖ and M represent, respectively, the total length of the train wagon, the first structural pulsation and the total mass of the structure. The vector field $[\mathbf{e}+v_T^2/(Rg)\mathbf{n}(s)]$ is assigned once the speed of the train and the curvature of the track are known; the attention is thus focused on the properties of the time–space function $p(s,\tau)$, physically representing the vertical component of the load.

2.1. Exact Fourier transform and relevant properties

As already remarked, if the speed of the train is assumed to be constant, the FT of expression (3) can easily be computed analytically. Indeed, since

$$\mathscr{F}[\delta(a+b\tau)] = \frac{1}{\sqrt{2\pi}|b|}\exp\left(\frac{\mathrm{i}a\omega}{b}\right), \quad b>0 \tag{4}$$

for the FT of the load (3) we will have

$$\begin{aligned} P(s,\omega) &= \mathscr{F}\left[\sum_{j=1}^{J} \Delta_j \delta(s_{0j}+\upsilon\tau - s)\right] \\ &= \frac{1}{\sqrt{2\pi}|\upsilon|}\sum_{j=1}^{J}\Delta_j \exp\left(\frac{\mathrm{i}(s-s_{0j})\omega}{\upsilon}\right), \quad \upsilon>0, \end{aligned} \tag{5}$$

i.e. a sum of complex numbers on the unit circle weighted by the dimensionless wheel forces Δ_j. Since, under a suitable temporal shift, two observers in two different abscissae (s_1 and s_2) measure the same time histories for the load, it is reasonable to expect that $P(s_1,\omega)$ and $P(s_2,\omega)$ share the same modulus while generally having a different phase. As a matter of fact it can easily be proven from Eq. (5) that the modulus $\|P(s,\omega)\|$ is independent of the abscissa s:

$$\begin{aligned} \Pi(\omega) &:= \|P(s,\omega)\| = \sqrt{P(s,\omega)P^*(s,\omega)} \\ &= \sqrt{\sum_{j,k}\frac{\Delta_j\Delta_k}{2\pi\upsilon^2}\exp\frac{\mathrm{i}(s-s_{0j})\omega}{\upsilon}\left[\exp\frac{\mathrm{i}(s-s_{0k})\omega}{\upsilon}\right]^*} \\ &= \frac{1}{\sqrt{2\pi}|\upsilon|}\sqrt{\sum_{j,k}\Delta_j\Delta_k\exp\left(\mathrm{i}\,\frac{(s_{0k}-s_{0j})\omega}{\upsilon}\right)}; \end{aligned} \tag{6}$$

where z^* denotes the complex conjugate of $z\in\mathbb{C}$. Hence, in problems of moving load identification (see for instance Ref. [17]), the modulus $\Pi(\omega)$ of the load can be measured on an arbitrary abscissa along the supporting structure and lead to the same response. The effect of the dimensionless train speed υ on the modulus (6) is twofold: while modulating $\Pi(\omega)$ through the term $1/|\upsilon|$ it also stretches the frequency scale through the term ω/υ. Thus, the shape of the modulus $\Pi(\omega)$ remains the same at different speeds provided the load and frequency scales are changed. On the contrary, the phase of the FT of the load

$$\varphi(s,\omega) := \arg P(s,\omega) = \arg\left[\sum_{j=1}^{J}\Delta_j\exp\left(\frac{\mathrm{i}(s-s_{0j})\omega}{\upsilon}\right)\right] \tag{7}$$

does depend on the abscissa s. Finally, using Eqs. (5)–(7), the FT of the load is usefully rewritten in polar form as

$$P(s,\omega) = \Pi(\omega)\exp[-\mathrm{i}\varphi(0,\omega)]\exp\left(\mathrm{i}\,\frac{\omega s}{\upsilon}\right); \tag{8}$$

the last exponential term in Eq. (8) represents the only term depending on the spatial coordinate s and will be called the load shape; the wavelength of the load shape equals $\lambda\equiv 2\pi\upsilon/\omega$ and is proportional to the velocity and inversely proportional to the frequency. Its contribution to the modal loads will become evident in the following sections.

2.2. Load projection on structural modes

The supporting structure is modelled here as a one-dimensional continuum; it is natural to assume that its domain is parametrized by the same abscissa s describing the track $\mathscr{C}$. Once the $\mathbb{R}^N$-valued function u has been defined, mapping every abscissa s and instant τ in the current kinematical descriptors, the dimensionless

equations governing the structural motion can be written as follows:

$$\begin{aligned} &\mathbf{L}[\mathbf{u}(s,\tau)] + \chi\dot{\mathbf{u}} + \ddot{\mathbf{u}} = \mathbf{T}(s)p(s,\tau), \quad s \in \mathscr{D} \coloneqq [0,\eta], \\ &\mathbf{B}[\mathbf{u}(s,\tau)] = 0, \quad s = 0,\eta \end{aligned} \tag{9}$$

with $\mathbf{L}$ being the linear self-adjoint stiffness operator, $\mathbf{B}$ representing the chosen boundary conditions, χ the dimensionless structural viscous damping, and $\mathbf{T}(s)$ an N-dimensional vector accounting for the track curvature and properly projecting the vertical load $p(s,\tau)$ onto the structural balance equations; to this aim $\mathbf{T}(s)$ is a suitable function of the vector field $[\mathbf{e} + v_T^2/(Rg)\mathbf{n}(s)]$ defined in Section 2. Here, a superimposed dot means the dimensionless time derivative while L_b is the length of the considered structure with $\eta \coloneqq L_b/L_w$ its dimensionless counterpart. The FT of Eq. (9) leads to

$$\mathbf{L}[\mathbf{U}(s,\omega)] + (\mathrm{i}\omega\chi - \omega^2)\mathbf{U}(s,\omega) = \mathbf{T}(s)P(s,\omega), \quad s \in \mathscr{D}. \tag{10}$$

By expanding the FT $\mathbf{U}(s,\omega)$ of the displacement in terms of the eigenfunctions $\mathbf{w}_m$ of $\mathbf{L}$ with boundary conditions as in Eq. (9):

$$\mathbf{U}(s,\omega) = \sum_m \mathbf{w}_m(s)U_m(\omega), \quad \begin{cases} \mathbf{L}[\mathbf{w}_m(s)] = \mu_m^2\mathbf{w}_m(s), & s \in \mathscr{D}, \\ \mathbf{B}[\mathbf{w}_m(s)]_{s=0,\eta} = 0 \end{cases} \tag{11}$$

for $m = 1, 2, \ldots$ we obtain

$$(\mu_m^2 + \mathrm{i}\omega\chi - \omega^2)U_m(\omega) = \int_0^\eta P(s,\omega)\mathbf{T}(s)\cdot\mathbf{w}_m(s)\,\mathrm{d}s =: \Psi_m(\omega), \tag{12}$$

where μ_m represents the mth structural pulsation and $\Psi_m(\omega)$ is the mth modal load. Recalling Eqs. (6) and (8), the polar components of $\Psi_m(\omega)$ are written as follows:

$$\begin{aligned} &\|\Psi_m(\omega)\| = \Pi(\omega)\left\|\int_0^\eta \exp\left(\mathrm{i}\,\frac{\omega s}{\upsilon}\right)\mathbf{T}(s)\cdot\mathbf{w}_m(s)\,\mathrm{d}s\right\|, \\ &\arg\Psi_m(\omega) = \arg\left(\int_0^\eta \exp\left(\mathrm{i}\,\frac{\omega s}{\upsilon}\right)\mathbf{T}(s)\cdot\mathbf{w}_m(s)\,\mathrm{d}s\right) - \varphi(0,\omega). \end{aligned} \tag{13}$$

Note that the difference between modal loads on different structural modes is only affected by the load shape $\exp(\mathrm{i}\omega s/\upsilon)$. Since both the functions $\mathbf{T}(s)\cdot\mathbf{w}_m(s)$ and $\exp(\mathrm{i}\omega s/\upsilon)$ are oscillating functions in $[0,\eta]$, the possible closeness of their spatial wavelengths could lead to a relevant scalar product in Eq. (13). Typically, the wavelengths of the modal shapes $\mathbf{w}_m(s)$ decrease as the mode number m increases; thus lower structural modes are prevalently loaded at lower values of the ratio ω/υ. This feature will be confirmed by the analytical predictions in Section 3 and by the numerical simulations in Section 4.

A final remark concerns the sequence of steps adopted to obtain the representation of the load (13); referring to the following diagram:

$$\begin{array}{ccc} & \langle\cdot,\,\mathbf{w}_m(s)\rangle & \\ \boxed{p(s,\,\tau)} & \longrightarrow & \boxed{\pi_m(\tau)} \\ \mathcal{F}\downarrow & & \mathcal{F}\downarrow \\ \boxed{P(s,\,\omega)} & \longrightarrow & \boxed{\Psi_m(\omega)} \\ & \langle\cdot,\,\mathbf{w}_m(s)\rangle & \end{array} \tag{14}$$

we first computed the FT $P(s,\omega)$ of the load $p(s,\tau)$ and then projected the results on the modes $\mathbf{w}_m$ to obtain the modal loads $\Psi_m(\omega)$. The diagram in Eq. (14) is commutative; in Appendix B proof is provided for a forcing time law $p(s,\tau)$ composed of a sum of Dirac delta functions. In the proof the time instants, in which each wheel enters and leaves the structural domain $[0,\eta]$, are used explicitly, even though, as expected, the final results $\Psi_m(\omega)$ are independent of them. Despite the commutativity of diagram (14), the alternative

path—often followed in the literature [17] and composed of a modal projection followed by a FT—turns out to be not convenient for several reasons:

- when forces are considered spatially lumped, as in the case of a sequence of train wheels, a large number of modes is needed for the convergence of $\sum \mathbf{w}_m(s)\pi_m(\tau)$ to $p(s,\tau)$;
- since the FT of $\pi_m(\tau)$ cannot be computed analytically, the computational effort is greatly increased; in addition, truncation and sampling errors are introduced;
- as far as travelling loads are concerned, the spatial and temporal steps should be related; hence, every time a non-uniform mesh is chosen for the spatial domain, special routines for computing the FT of an unevenly sampled set of data are needed.

3. Simplified analytic solutions

In the expressions obtained, sums over the number of the train wheels are involved, the information about the train characteristics being gathered into the lists $\{\Delta_j,\ j=1,\dots J\}$ and $\{s_{0j},\ j=1,\dots J\}$. In order to extract from these data expressive analytical information regarding the dynamic load of the train, it is useful to introduce some simplifying hypotheses.

According to Fig. 1, the weight of the whole train is assumed to be distributed uniformly over asset of equally spaced wheels, the constant distance between these wheels being the length L_w of the wagon. In Fig. 1, two steps are necessary to proceed from the actual configuration of the train wheels (a), in which several characteristic lengths are needed for description, to the simplest configuration (c) in which only one characteristic length is present. One could choose either the first wheel of each wagon, as sketched in Fig. 1, or, equivalently, the center of mass of the wheels in each wagon in order to proceed from the actual to the simplest configuration; the difference between the two choices is indeed only a temporal shift. Having chosen the characteristic length of the wagon as the unit length, the hypothesis discussed is equivalent to assuming that:

$$s_{0j} \to (1-j), \quad \Delta_j \to Q/N_w, \quad j=1,2,\dots \equiv N_w \tag{15}$$

with Q the dimensionless weight of the whole train and $N_w = J/4$ the number of wagons, including the locomotives. Note that L_w is also the most frequently occurring value in the differences $(s_{0k}-s_{0j})$ involved in Eq. (6): this observation suggests how further to improve the above hypothesis. Indeed, by inspecting the table of numbers $\{(s_{0k}-s_{0j}),\ k,\ j=1,2,\dots J\}$ one can find an ordered sequence of the "most frequent" lengths and use these to generate sets of uniformly spaced sequences of point loads approximating the actual train: for instance, the configuration (b) in Fig. 1 represents the best approximation of the actual train (a) based on two characteristic lengths, respectively, labelled as L_w and δ. However, since manageable and synthetic expressions

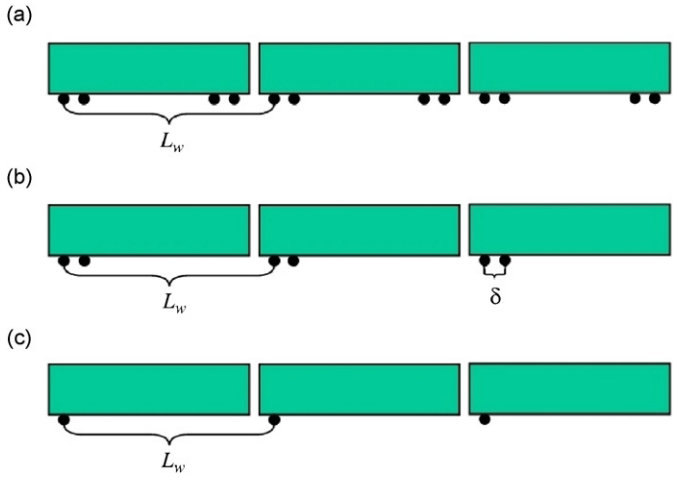

Fig. 1. Exact and simplified descriptions of the train parameters: (a) exact sequence, (b) approximating sequence with two characteristic lengths and (c) approximating sequence with one characteristic length.

are sought, the attention is limited to the simplest case of assumption (15) in which only one characteristic length is retained.

3.1. Reduced expressions of the load modulus and phase

Using the previous hypothesis, the modulus of the FT of the load, $\Pi(\omega)$ in Eq. (6), reduces to

$$\hat{\Pi}(\omega) = \frac{Q}{N_w\sqrt{2\pi}|v|}\sqrt{\sum_{j,k}^{N_w}\exp\left(\mathrm{i}\,\frac{(j-k)\omega}{v}\right)} = \frac{Q}{\sqrt{2\pi}|v|}\left|\frac{\sin\dfrac{N_w\omega}{2v}}{N_w\sin\dfrac{\omega}{2v}}\right|, \tag{16}$$

while its phase, $\varphi(s,\omega)$ in Eq. (7), reduces to

$$\hat{\varphi}(s,\omega) = \arg\left[\sum_{j=1}^{N_w}\exp\left(\frac{\mathrm{i}(s-1+j)\omega}{v}\right)\right] = \left.\frac{(N_w+2s-1)\omega}{2v}\right|_{\mathrm{mod}(2\pi)}; \tag{17}$$

here and in the following the superimposed hat means the approximated value of the quantities, in accordance with assumption (15).

In Fig. 2 the function $|\sin N_w\beta|/|N_w\sin\beta|$ is plotted as a function of the parameter $\beta = \omega/(2v) = L_w\omega\varpi/(2v_T)$ for $N_w = 6$. This function is bounded by 1, is periodic of period π and has global maxima in the points $\beta = n\pi$, $n = 0, 1, \ldots$; in each period there are exactly $(N_w - 1)$ peaks.

Hence according to hypothesis (15), the modulus $\|P(s,\omega)\|$ of the load FT has its highest values, namely $Q/(\sqrt{2\pi}|v|)$, centered at $\beta = n\pi$, or, in terms of dimensional quantities, at the frequencies:

$$\bar{f}_n \coloneqq nv\varpi = n\frac{v_T}{L_w}, \quad n = 1, 2\ldots\ . \tag{18}$$

Hence, the characteristic frequencies of the load are multiples of the ratio between the speed of the train and the length of the wagon. Let us stress the linear dependence of the frequency peaks (18) on the speed of the train, since this linear correspondence will be exploited in the following sections. The exact description (6) for the load comprising a non-uniform, unevenly spaced sequence of point loads can, of course, contain several other harmonics: those listed in Eq. (18) correspond to the dominant terms. It is worth noting that, at the nth critical frequency (18), the wavelength of the load shape $\lambda = 2\pi v/\omega$ equals $1/n$, or in terms of dimensional quantities L_w/n.

3.2. Bounds for the structural response

In this section, we derive some bounds for the structural response regardless of whether the structural eigenfunctions are known; in Section 4.1, the structural response will instead be evaluated through the modal projection of the load shape as in Eq. (13).

The bounds for both the modal loads and responses are derived from expressions (16) and (17). After their substitution in Eq. (13), one easily obtains

$$\|\hat{\Psi}_m(\omega)\| \leqslant \hat{\Pi}(\omega)\|\mathbf{w}_m\|\|\mathbf{T}\|\left\|\int_0^{\eta}\exp[\mathrm{i}\hat{\varphi}(s,\omega)]\,\mathrm{d}s\right\|; \tag{19}$$

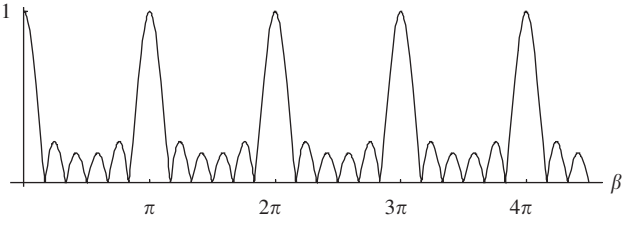

Fig. 2. Plot of the function $|\sin N_w\beta|/|N_w\sin\beta|$ as a function of β for $N_w = 6$.

the last integral can be estimated through Eq. (17) to obtain

$$\left\| \int_0^{\eta} \exp\left[\mathrm{i} \, \frac{(N_w + 2s - 1)\omega}{2\upsilon} \right] \mathrm{d}s \right\| = \frac{\sqrt{2}\upsilon}{\omega} \sqrt{1 - \cos\frac{\omega\eta}{\upsilon}}. \tag{20}$$

Thus, using an orthonormal system of eigenfunctions, one ends up with the following bounds for the moduli of the FT of the modal loads:

$$\|\hat{\Psi}_m(\omega)\| \leqslant \frac{Q\|\mathbf{T}\|}{\sqrt{\pi}\omega} \left| \frac{\sin\dfrac{N_w\omega}{2\upsilon}}{N_w \sin\dfrac{\omega}{2\upsilon}} \right| \sqrt{1 - \cos\frac{\omega\eta}{\upsilon}}. \tag{21}$$

Let us explicitly note that the limit $\lim_{\omega\to 0} \|\hat{\Psi}_m\| \leqslant Q\|\mathbf{T}\|\eta/(\sqrt{\pi}\upsilon)$ is finite. As a consequence of Eq. (21), the bounds for the structural response in terms of moduli of the Fourier coefficients $U_m(\omega)$ are immediately derived from Eq. (12) to obtain

$$\|\hat{U}_m(\omega)\| = \frac{\|\Psi_m(\omega)\|}{\sqrt{(\mu_m^2 - \omega^2)^2 + \omega^2\chi^2}} \leqslant \frac{Q\|\mathbf{T}\|}{\sqrt{\pi}\omega\sqrt{(\mu_m^2 - \omega^2)^2 + \omega^2\chi^2}} \left| \frac{\sin\dfrac{N_w\omega}{2\upsilon}}{N_w \sin\dfrac{\omega}{2\upsilon}} \right| \sqrt{1 - \cos\frac{\omega\eta}{\upsilon}}. \tag{22}$$

Thus the static modal responses are bounded by

$$\lim_{\omega\to 0} \|\hat{U}_m(\omega)\| \leqslant \frac{Q\|\mathbf{T}\|\eta}{\sqrt{\pi}\upsilon\mu_m^2}, \tag{23}$$

whilst the responses at the structural resonant frequencies are bounded by

$$\lim_{\omega\to\mu_m\pm\frac{\chi}{2}} \|\hat{U}_m\| \leqslant \frac{\sqrt{2}Q\|\mathbf{T}\|}{\sqrt{\pi}(\chi\mu_m)^{3/2}} \left| \frac{\sin\dfrac{N_w\mu_m}{2\upsilon}}{N_w \sin\dfrac{\mu_m}{2\upsilon}} \right| \sqrt{2 - 2\cos\frac{\mu_m\eta}{\upsilon}}. \tag{24}$$

Eq. (24) enables optimal values for the speed of the train to be found in order to produce the minimal structural response. Indeed, referring to Fig. 2, where the function $|\sin N_w\beta|/|N_w \sin\beta|$ was plotted, the structural response (24) is minimized when both the function:

$$|[\sin(N_w\mu_m)/(2\upsilon)]/[N_w \sin\mu_m/(2\upsilon)]| \tag{25}$$

and its envelope have minima, i.e. when

$$\frac{\mu_m}{\upsilon} = (2k+1)\pi \quad \text{or} \quad \upsilon = \frac{\mu_m}{(2k+1)\pi}. \tag{26}$$

For $k = 1, 2, \ldots$ Eq. (26) yields the less critical values of the speed of the train for the mth structural mode.

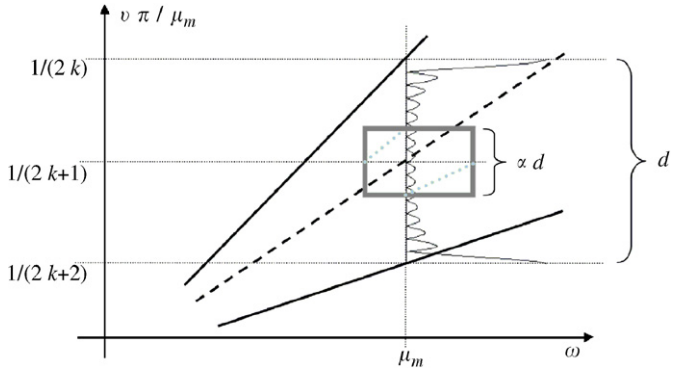

Fig. 3. Maximum allowed variance of speed optimal values.

In Fig. 3 the traces of the maxima (solid black) and minima (dashed black) of the function (25) are drawn, for $N_w = 16$, on the frequency–speed plane $(\omega, \upsilon\pi/\mu_m)$. Accordingly, a procedure to derive the maximum allowed variance of the optimal values (26) is established; the main assumption is to limit the velocity in a fraction, say $\alpha < 1$, of the region between two successive maxima. After some algebra, the optimal values for the dimensionless speed in order to produce the minimum response on the mth mode are given by the following intervals:

$$\upsilon^{\text{opt}} = \frac{\mu_m}{\pi}\left\{\frac{1}{2k+1} - \frac{1}{4k\alpha(k+1)}, \frac{1}{2k+1} + \frac{1}{4k\alpha(k+1)}\right\}_{k=1,2,\ldots}. \tag{27}$$

In Section 4.2, formula (27) will be tested on the numerical solution of a real problem, namely the determination of the optimal range of speed for the train ETR500 travelling on a single-span bridge.

4. Comparisons between analytical and numerical results

4.1. Benchmark solution: beam on elastic foundation

Although several kinds of boundary condition could naturally be considered, a simply supported straight Euler beam on an elastic foundation is here solved analytically in order to obtain a benchmark solution. In this case the closed form expression of the structural eigenfunctions $\mathbf{w}_m(s)$ allows for an exact estimation of the modal loads and responses, rather than the inequalities (19) and (24) obtained for unknown eigenfunctions.

Once the dimensionless space and time variables as given in Eq. (2) are chosen, the equations of motion (9) are rewritten

$$\frac{\eta^4}{\pi^4}u^{IV} + \underbrace{\frac{kL_b^4}{\pi^4 EI}}_{\kappa}u + \underbrace{\frac{cL_b^2}{\pi^2}\sqrt{\frac{L_b}{MEI}}}_{\chi}\dot{u} + \ddot{u} = \sum_{j=1}^{J} \Delta_j \delta(s_{0j} + \upsilon\tau - s) \quad \text{on } [0,\eta], \tag{28}$$

where $u = w/L_b$ is the dimensionless transverse displacement, EI is the bending stiffness, k is the elasticity of the ground and c is a damping factor. In deriving Eq. (28) the characteristic pulsation ϖ has been chosen as the first natural frequency of the simply supported beam with a vanishing elasticity ground ($k = 0$, $c = 0$), i.e. $\varpi = (\pi^2/L_b^2)\sqrt{EIL_b/M}$; accordingly, the dimensionless weights (2) of the train wheels are also expressed by $\Delta_j = W_j L_b^3/(\pi^4 EIL_w)$. By comparing Eq. (9) with Eq. (28), the explicit expression of the operator L in Eq. (9) and its eigenvalues and normalized eigenfunctions are derived:

$$L[u] = \frac{\eta^4}{\pi^4}u^{IV} + \kappa u, \quad \mu_m^2 = m^4 + \kappa, \quad \mathbf{w}_m(s) = \sqrt{\frac{2}{\eta}}\sin\frac{m\pi s}{\eta}, \tag{29}$$

while the vector $\mathbf{T}$ reduces to the vector $\{\mathbf{e}\cdot\mathbf{e} = 1\}$, since $R \to \infty$. The expression for the polar form of the modal loads $\Psi_m(\omega)$ can now be computed through assumption (15); indeed, using Eqs. (17) and (29), Eq. (13) for the moduli of the FT of the modal loads simplifies to

$$\begin{aligned}\|\hat{\Psi}_m(\omega)\| &= \hat{\Pi}(\omega)\left\|\int_0^{\eta}\exp\left[\frac{\mathrm{i}(N_w+2s-1)\omega}{2\upsilon}\right]\sqrt{\frac{2}{\eta}}\sin\frac{m\pi s}{\eta}\,\mathrm{d}s\right\| \\ &= \hat{\Pi}(\omega)\frac{2\sqrt{2\eta}m\pi\upsilon^2}{|\eta^2\omega^2 - m^2\pi^2\upsilon^2|}\left|\sin\frac{m\pi + \frac{\eta\omega}{\upsilon}}{2}\right|.\end{aligned} \tag{30}$$

Finally, for the moduli of the Fourier coefficients of the response, one easily obtains

$$\|\hat{U}_m(\omega)\| = \frac{2\sqrt{\pi\eta}\, m\upsilon Q}{\sqrt{(m^4+\kappa-\omega^2)^2+\omega^2\chi^2}} \left|\frac{\sin\dfrac{N_w\omega}{2\upsilon}}{N_w \sin\dfrac{\omega}{2\upsilon}}\right| \left|\frac{\sin\dfrac{m\pi+\dfrac{\eta\omega}{\upsilon}}{2}}{\eta^2\omega^2-m^2\pi^2\upsilon^2}\right|. \tag{31}$$

The static response of the bridge, i.e. the response for $\omega \to 0$, is essentially described by the first mode; indeed, since

$$\|\hat{U}_m(0)\| = \frac{2\sqrt{\pi\eta}\, Q}{m\pi^2\upsilon(m^4+\kappa)} \left|\sin\frac{m\pi}{2}\right|, \tag{32}$$

then $\|\hat{U}_1(0)\| \gg \|\hat{U}_3(0)\| \gg \|\hat{U}_5(0)\|$ and $\|\hat{U}_m(0)\| = 0$ for m even.

The maxima of the function $\|\hat{U}_m(\omega)\|$ in Eq. (31), in the dynamic regimes, are instead obtained when these coefficients are evaluated at the associated eigenfrequencies, i.e. for $\omega \to \mu_m = \sqrt{m^4+\kappa}$. The resulting expression $\lim_{\omega\to\mu_m}\|\hat{U}_m\|$ is given by the multiplication of three terms:

$$\|\hat{U}_m\|_{\max} = \frac{2\sqrt{\pi}mQ}{\mu_m\chi} \left|\frac{\upsilon\sqrt{\eta}}{\eta^2\mu_m^2-m^2\pi^2\upsilon^2}\right| \left|\frac{\sin\dfrac{N_w\mu_m}{2\upsilon}}{N_w\sin\dfrac{\mu_m}{2\upsilon}}\right| \left|\sin\frac{m\pi+\dfrac{\eta\mu_m}{\upsilon}}{2}\right|. \tag{33}$$

Once the speed values $\upsilon^*_{i=1,2,3}$ have been defined

$$\begin{aligned} &\upsilon_1^*(\eta) \coloneqq \frac{\eta\mu_m}{\pi m}, \quad \upsilon_{2n}^* \coloneqq \frac{\mu_m}{2n\pi}, \quad n = 1,2,\ldots, \\ &\upsilon_{3k}^*(\eta) \coloneqq \frac{\mu_m\eta}{(2k+1-m)\pi}, \quad k = 1,2,\ldots\ . \end{aligned} \tag{34}$$

critical, respectively, for each of the three terms in Eq. (33), the maximal structural response of the mth mode occurs at the possible intersections of the three curves $\upsilon^*_{i=1,2,3}(\eta)$ in the plane (η,υ).

The second critical condition $\upsilon \equiv \upsilon_2^*(\eta)$ has already been discussed, see Eq. (18), and occurs when the ratio v_T/L_w between the speed of the train and characteristic wagon length is a multiple of one structural frequency; in this case the load modulus $\Pi(\omega)$ is resonant with the structural mode considered. The other two contributions are instead related to the projections of the load shape (8) onto the structural eigenfunctions. Indeed, when $\upsilon \equiv \upsilon_1^*(\eta)$ and $\omega \equiv \mu_m$ the load shape wavelength ($\lambda = 2\pi\upsilon/\omega = 2\eta/m$) coincides with the mth modal wavelength, see Eq. (29), whilst in the critical sets $\upsilon \equiv \upsilon_{3k}^*(\eta)$ the load shape wavelength equals suitable fractions of the modal wavelengths. Hence, the simultaneous occurrence of the first and second critical conditions in Eq. (34), i.e. the intersections of curves $\upsilon_1^*(\eta)$ and υ_{2n}^*, indicates a load characterized by both the same frequency and the same wavelength as the considered mode. This worst case is more often encountered for short span bridges: as a matter of fact, in order to have $\upsilon_1^*(\eta) = \upsilon_{2n}^*$ for the mth structural mode, one needs $L_b \leqslant mL_w/2$, meaning a bridge length less than $m/2$ the length of the wagon.

The overall scenario is depicted in Fig. 4 where the maximal response $\|\hat{U}_1\|_{\max}$ of the first structural mode has been plotted on the plane (η,υ). The sets of critical speeds $\upsilon_1^*(\eta)$, $\{\upsilon_{2n}^*\}$ and $\{\upsilon_{3k}^*(\eta)\}$ are also plotted by a dashed black line, a set of solid black lines and a set of dotted gray lines, respectively. With $L_w \simeq 15-30\,\mathrm{m}$, typical values for the parameter η range from 0.5 up to 4, whilst the parameter υ can vary from 0 up to 0.4 ($L_w \simeq 15\,\mathrm{m}$, $v_T \simeq 270\,\mathrm{km/h}$, $\varpi/2\pi \simeq 2\,\mathrm{Hz}$). The tendency is to have the highest structural responses in the region of low values of the parameter η, namely short span bridges, and in the region near the first critical speed υ_{21}^* (resonant load condition); outside these regions the structural response is noticeably lower. The usefulness of the results described is twofold: indeed, given a bridge whose span length and first natural frequency are L_b and ϖ, one can find the optimal speeds for a given train, with wagons of length L_w, in order to minimize the response. Similarly, given the speed of the train considered, one can find several intervals for choosing the optimal lengths of the bridge span. It is useful to recall that Eq. (31), from which the above discussion follows, represents the exact solution for the case of a simply supported, elastically grounded beam,

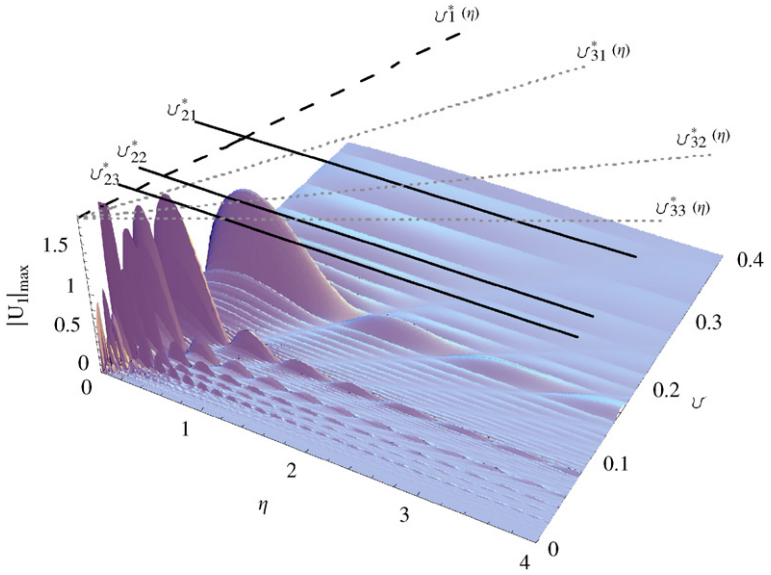

Fig. 4. Maximal response $\|\hat{U}_1\|_{\max}$ of the first structural mode on the (η, υ) plane.

Table 1
Numerical data used in the simulations

Bridge	$L_b = 70\,\text{m}$, $\mu_1/2\pi = 2.51\,\text{Hz}$, $\mu_2/2\pi = 2.75\,\text{Hz}$, $M = 1.8 \times 10^7\,\text{kg}$
Train	$L_w = 26.1\,\text{m}$, $N_w = 12$, $\sum_j^J W_j = 6.2 \times 10^5\,\text{kg}$ (total weight)

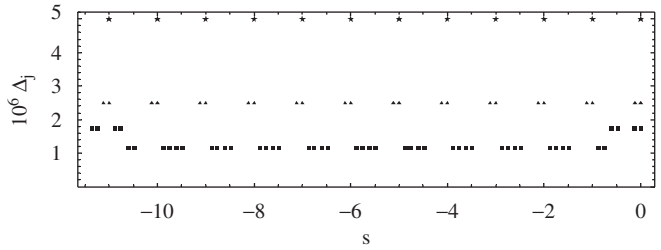

Fig. 5. Sequences of weights for the ETR500: actual train (squares), approximating sequences with one characteristic length (stars) and two characteristic lengths (triangles).

subjected to a uniform and regularly spaced sequence of N_w point loads; in general, it only gives a conservative approximation of the true solution (8) through assumption (15), as underlined in the application of the next section.

4.2. High-speed train on a single span arched bridge

The case of a high-speed train, namely an ETR500, over a single-span arched bridge is used to compare results between the exact, numerically computed, expressions of $\Pi(\omega)$, $\Psi_m(\omega)$, $U_m(\omega)$ and their analytical approximations $\hat{\Pi}(\omega)$, $\hat{\Psi}_m(\omega)$, $\hat{U}_m(\omega)$ through the assumption (15). The bridge under consideration is characterized by having the first two natural frequencies very close together; nevertheless, for the first four

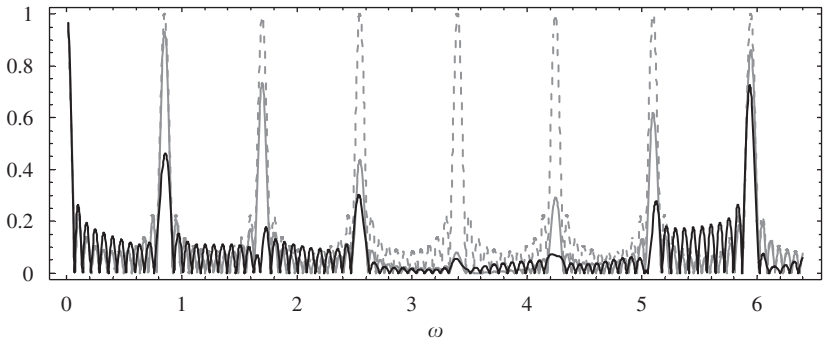

Fig. 6. FT of the loads associated to the ETR500 sequences as function of frequency ($v_T = 200\,\mathrm{km/h}$). Actual train (solid black), approximating sequences with one characteristic length (dashed gray) and two characteristic lengths (solid gray).

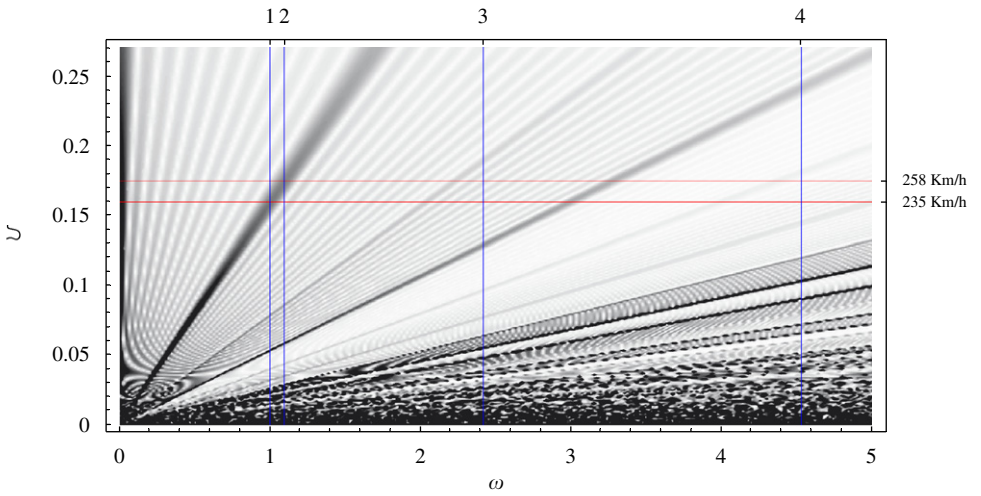

Fig. 7. Π as a function of ω and υ; darker zones indicate higher values of the function. The vertical lines correspond to the first four natural frequencies of the structure.

frequencies, the modal shapes of the bridge closely follow the modes of a simply supported beam; in particular the first mode is symmetric whilst the second is antisymmetric with respect to the beam midpoint. Table 1 collects the main numerical data concerning the bridge and the train under consideration.

In Fig. 5, the actual sequence of weight point loads relative to the ETR500 train is plotted together with its uniform and equally spaced approximations with one (star-shaped symbols) and two (triangle-shaped symbols) characteristic lengths; refer, respectively, to Figs. 1(c) and (b). The corresponding moduli of the FT of the loads associated with these sequences of travelling point loads are drawn in Fig. 6. As already discussed, the exact solution (solid black line) is bounded at the critical frequencies by both approximations with one (dashed gray line) and two (solid gray line) characteristic lengths. The approximation with two characteristic lengths also describes the modulation with frequency v_T/δ of the highest peaks, whose positions are multiples of the ratio v_T/L_w. As a matter of fact, a phenomenon similar to frequency modulation takes place between the two leading harmonic terms characterized by the two close frequencies v_T/L_w and $v_T/(L_w+\delta)$. The moduli of the FT of the load, both the exact (5) and the approximated analytic expression (17), are also displayed as functions of ω and υ by two contour plots in Figs. 7 and 8, respectively. A comparison of these figures shows a significant agreement between the exact Π and approximated $\hat{\Pi}$ shapes of the FT of the load. The main differences are represented by an overestimation of the load $\hat{\Pi}$ along some lines of the (ω, υ) plane; as already discussed, the approximation (15) leads to a simplified but more conservative model for the train load.

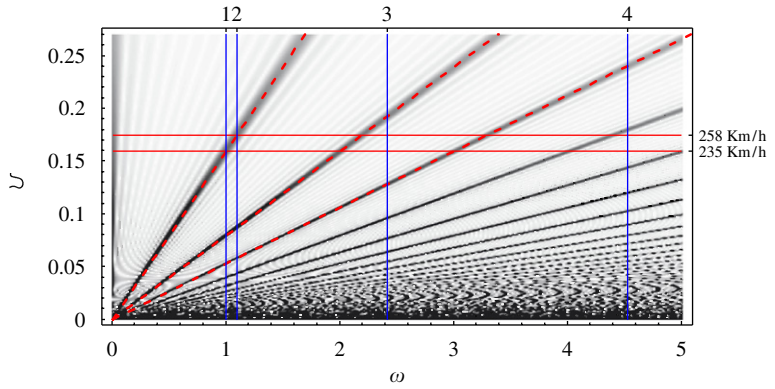

Fig. 8. $\hat{\Pi}$ as a function of ω and υ; darker zones indicate higher values of the function. The vertical lines correspond to the first four natural frequencies of the structure.

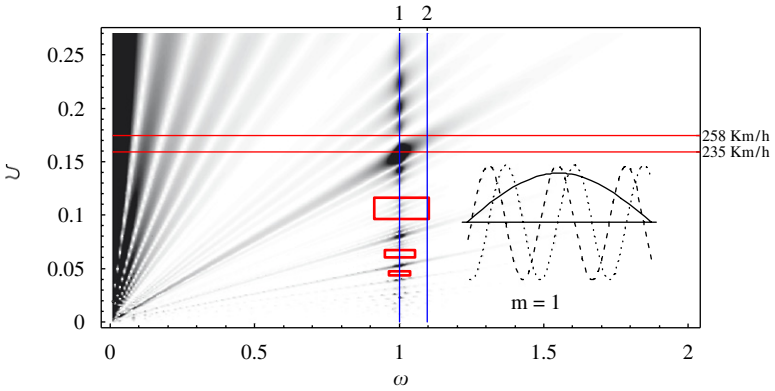

Fig. 9. $\|U_1\|$ as a function of ω and υ. The vertical lines correspond to the first two natural frequencies, the horizontal lines and the rectangles indicate the analytical predictions for respectively the critical values and the optimal ranges of train speed.

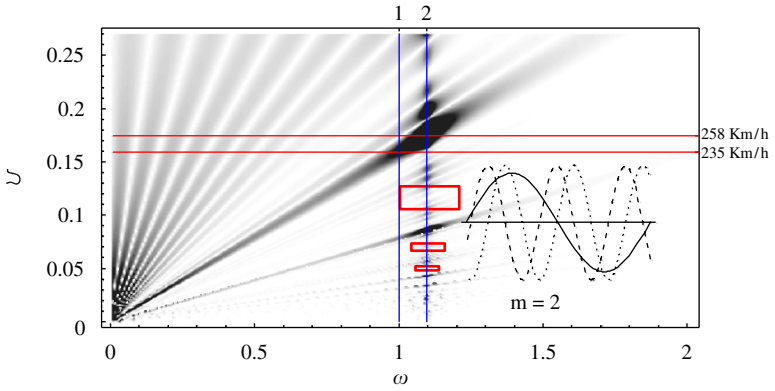

Fig. 10. $\|U_2\|$ as a function of ω and υ. The vertical lines correspond to the first two natural frequencies, the horizontal lines and the rectangles indicate the analytical predictions for respectively the critical values and the optimal ranges of train speed.

Despite the difference in the maximal values of the load, the simplified model is able to predict correctly not only the overall qualitative response, but also the critical conditions of the main parameters (dimensionless frequency and speed). Indeed, in Figs. 7 and 8 the critical speeds for the first two modes of the considered

Table 2
Train speed ranges (km/h) for the first three modes minimal response

Mode 1	157 ± 14	94 ± 5	67 ± 2	52 ± 2	43 ± 1
2	172 ± 16	103 ± 5	74 ± 3	57 ± 2	47 ± 1
3	380 ± 35	228 ± 12	163 ± 6	127 ± 3	104 ± 2

bridge are emphasized by two horizontal lines. The exact values coincide with the approximated values as found by Eq. (18); in both cases the dimensional train speeds equal the products of the length of the wagon with the structural frequencies, leading, respectively, to 235 and 258 km/h.

Figs. 9 and 10, in which the moduli of the first two modal responses are drawn on the plane (ω, υ), confirm these analytical predictions, showing the highest amplitudes at the predicted train speeds. In both figures, the structural modal shapes and the real and imaginary parts of the load shape $\exp[i(\omega s/\upsilon - \varphi(0,\omega))]$ are plotted with solid, dashed and dotted lines, respectively. For the considered bridge, the wavelengths of the first and second modes are, respectively, equal to $2L_b \simeq 140$ m and $L_b \simeq 70$ m, whilst, as discussed in Section 3.1, at the first ($n = 1$) critical speed the wavelength of the load shape equals the total length of the wagon $L_w \simeq 26$ m; hence, at the critical points the two modal shapes are close to being orthogonal to the load shape (89.0° and 86.5° angles, respectively).

Since the first two natural frequencies are close, the speeds needed for their resonances are also close; meanwhile the wavelength of the second mode is twice the wavelength of the first mode, and, as such, more similar to the load wavelength. This explains the relevant contribution of the second mode to the structural dynamic response. Although the load and modal shapes are close to being orthogonal, the resonance condition is nonetheless able to produce dynamic effects with the same order of magnitude as the static response. As predicted by Eq. (32), the static response is essentially given by the first mode contribution.

Finally, Eqs. (18) and (27) are used to derive the ranges of train speed leading to the minimal response of a given structural mode, together with their maximum allowed tolerance. These optimal values are listed in Table 2 for the first 3 structural modes and are confirmed by the numerical results in Figs. 9 and 10, where, the gray rectangles correspond to the first three optimal frequency–speed ranges, analytically derived in Eq. (27).

5. Conclusions

The structural load due to train passages is studied from an analytical viewpoint; to this end, some simplifying hypotheses are introduced and discussed. By neglecting the interaction between the train and the structure and reducing the parameters describing the composition of the train, a coarse, more conservative model for the dynamic load acting on the structure is derived. Exact analytic solutions for the case of equally spaced and uniform sequences of travelling point loads are found; a general procedure to reduce any train to this kind of sequence, whilst preserving the essential features of its dynamic load, is also introduced. The main features of the Fourier transform (FT) of the load are enlightened: the independence of the load modulus in relation to the abscissa on the track, the behavior of the load frequency peaks in relation to the composition and speed of the train, and some bounds for the structural response to sequences of moving loads.

For bridge structures with separate natural frequencies, the first mode contributes mainly to the structural response, since the resonance condition typically requires too high speeds; an arched bridge is referred to, for which the second mode contribution is also relevant due to the closeness of the first two natural frequencies.

Despite their simplicity, these results represent useful tools to derive the main choices for both structural design and health monitoring tests with manageable expressions for the critical ranges of both the structural eigenfrequencies and train speeds. For instance, the expressions of the FT of the load represent fundamental tools for extracting the structural frequency-response function from forced vibration data of structures subjected to railway traffic. Indeed, since the railway traffic load is characterized by a set of characteristic frequency peaks, a suitable deconvolution procedure, based on the analytic knowledge of the load FT, should be developed.

Appendix A

In the developed model the inertia of the masses travelling over the structure has been intentionally neglected; here, the limit of validity of this assumption is estimated.

To this end, consider the wheels—the dimensionless mass of which are labelled as $v_j = \varpi^2 L_w \Delta_j / g$—as a set of oscillators travelling along the structure; these kinds of problem are considered for instance in Refs. [14,18]. If, for the sake of simplicity, the structure is supposed to be modelled as an Euler beam, the equations of motion read as follows:

$$\begin{aligned} &v_j \ddot{y}_j + h[y_j - u(s_{0j} + \upsilon\tau, \tau)] = \Delta_j, \quad j = 1, \ldots, J, \\ &\frac{\eta^4}{\pi^4} u^{IV} + \kappa u + \chi \dot{u} + \ddot{u} = \sum_{j=1}^{J} h[y_j - u(s_{0j} + \upsilon\tau, \tau)]\delta(s_{0j} + \upsilon\tau - s), \end{aligned} \tag{35}$$

where y_j is the dimensionless vertical displacement of the jth wheel and h its dimensionless stiffness; the meaning of the remaining symbols in Eq. (35) are the same as in Eq. (28). If these oscillators are supposed to be vertically clamped on the structure, in other words if $y_j \longrightarrow u(s_{0j} + \upsilon\tau, \tau)$, then for the vertical acceleration of the masses, by deriving twice with respect to time τ, the expression

$$u(s_{0j} + \upsilon\tau, \tau) = \int_{-\infty}^{\infty} u(s, \tau)\delta(s_{0j} + \upsilon\tau - s)\,\mathrm{d}s, \tag{36}$$

we obtain

$$\ddot{y}_j \longrightarrow \ddot{u}(s_{0j} + \upsilon\tau, \tau) + 2\upsilon\dot{u}'(s_{0j} + \upsilon\tau, \tau) + \upsilon^2 u''(s_{0j} + \upsilon\tau, \tau). \tag{37}$$

Hence, Eq. (35) is rewritten

$$\begin{aligned} &\frac{\eta^4}{\pi^4} u^{IV} + \kappa u + \upsilon^2 \sum_j v_j u''(s_{0j} + \upsilon\tau, \tau)\delta(s_{0j} + \upsilon\tau - s) \\ &\quad + \chi\dot{u} + 2\upsilon \sum_j v_j \dot{u}'(s_{0j} + \upsilon\tau, \tau)\delta(s_{0j} + \upsilon\tau - s) \\ &\quad + \ddot{u} + \sum_j v_j \ddot{u}(s_{0j} + \upsilon\tau, \tau)\delta(s_{0j} + \upsilon\tau - s) = \sum_j \Delta_j \delta(s_{0j} + \upsilon\tau - s) \end{aligned} \tag{38}$$

or, after a standard Galerkin projection on a set of normalized modes ($u(s, \tau) = \sum_m w_m(s) u_m(\tau)$):

$$\begin{aligned} &\left[\mu_n^2 \delta_{nm} + \upsilon^2 \sum_{j,n} v_j w_m''(s)\Big|_{s=s_{0j}+\upsilon\tau} w_n(s_{0j} + \upsilon\tau)\right] u_m \\ &\quad + \left[\chi\delta_{nm} + 2\upsilon \sum_{j,n} v_j w_m'(s)\Big|_{s=s_{0j}+\upsilon\tau} w_n(s_{0j} + \upsilon\tau)\right] \dot{u}_m \\ &\quad + \left[\delta_{nm} + \sum_{j,n} v_j w_m(s_{0j} + \upsilon\tau) w_n(s_{0j} + \upsilon\tau)\right] \ddot{u}_m = \sum_j \Delta_j \delta(s_{0j} + \upsilon\tau - s). \end{aligned} \tag{39}$$

It can immediately be seen that the travelling masses make the resulting system linear, but with time-varying coefficients; if an averaging procedure is applied to the time-varying terms, the effect is still to couple all the modes through elastic, viscous and inertial additional matrices. Thus, for our purposes, Eq. (39) is too difficult to derive analytical information; however, it can be used to estimate the limits within which the additional terms due to travelling masses can be neglected. Indeed, since the eigenfunctions are bounded by the normalizing conditions, the relative importance of these additional terms can be coarsely bounded by the

following ratios:

$$\left(v^2\sum_j v_j\right)\Big/\mu_n^2,\quad \left(2v\sum_j v_j\right)\Big/\chi,\quad \left(\sum_j v_j\right)\Big/1. \tag{40}$$

Hence, when all three upper bounds are sufficiently small, the time-varying terms can be neglected or, for greater accuracy, averaged over the modal periods; in the case of an ETR500 train, the values 0.1%, 0.5%, and 3.5% were respectively obtained for the three bounds in the worst case $n = 1$, and the associated time-varying contributions to the motion equations were therefore neglected.

Appendix B. Commutativity of diagram (14)

Claim. *Given* $p(s,\tau) \coloneqq \sum_{j=1}^{J} \Delta_j \delta(s_{0j} + v\tau - s)$, *then*:

$$\langle \mathscr{F}[p(s,\tau)], w(s)\rangle = \mathscr{F}[\langle p(s,\tau), w(s)\rangle] \tag{41}$$

for every function $w(s)$ *vanishing outside the interval* $[0,\eta]$.

Proof. Using the well-known Fourier transform of a travelling Dirac delta (4) we obtain, for the RHS of Eq. (41):

$$\begin{aligned}\langle \mathscr{F}[p(s,\tau)], w(s)\rangle &= \left\langle \mathscr{F}\left[\sum_{j=1}^{J}\Delta_j\delta(s_{0j}+v\tau-s)\right], w(s)\right\rangle \\ &= \frac{1}{\sqrt{2\pi}|v|}\sum_{j=1}^{J}\Delta_j\left\langle e^{-\frac{i(s-s_{0j})\omega}{v}}, w(s)\right\rangle \\ &= \frac{1}{\sqrt{2\pi}|v|}\sum_{j=1}^{J}\Delta_j\int_0^{\eta} e^{\frac{-i(x-s_{0j})\omega}{v}} w(x)\,dx.\end{aligned} \tag{42}$$

To evaluate the LHS of Eq. (41) we need first to compute the projection $\langle p(s,\tau), w(s)\rangle$ and then computing the FT of the resulting time function. Since the function $w(s)$ vanishes outside the interval $[0,\eta]$, it can always be regarded as the product

$$w(s) \coloneqq \hat{w}(s)\chi(s),\quad \chi(s) \coloneqq \begin{cases} 0, & s<0,\ \text{or } s>\eta,\\ 1 & 0\leqslant s\leqslant\eta.\end{cases} \tag{43}$$

$\hat{w}(s)$ being defined with no restrictions on all the real axis. Hence

$$\begin{aligned}\langle p(s,\tau), w(s)\rangle &= \sum_{j=1}^{J}\Delta_j\int_0^{\eta}\delta(s_{0j}+v\tau-s)w(s)\,ds \\ &= \sum_{j=1}^{J}\Delta_j\hat{w}(s_{0j}+v\tau)\chi(s_{0j}+v\tau).\end{aligned} \tag{44}$$

The time functions $\chi(s_{0j}+v\tau)$ vanish everywhere except in the intervals $T_{j1}\leqslant\tau\leqslant T_{j2}$ when $\chi(s_{0j}+v\tau)=1$; here $T_{j1} \coloneqq s_{0j}/v$, and $T_{j2} \coloneqq (s_{0j}+\eta)/v$ are the instants at which the jth wheel enters and leave the domain $[0,\eta]$.

Finally for the LHS of Eq. (41), we obtain

$$\begin{aligned}\mathscr{F}[\langle p(s,\tau), w(s)\rangle] &= \frac{1}{\sqrt{2\pi}}\int_{-\infty}^{+\infty}\left[\sum_{j=1}^{J}\Delta_j\hat{w}(s_{0j}+\upsilon\tau)\chi(s_{0j}+\upsilon\tau)\right]\mathrm{e}^{-\mathrm{i}\omega\tau}\,\mathrm{d}\tau\\ &= \frac{1}{\sqrt{2\pi}}\sum_{j=1}^{J}\Delta_j\int_{-\infty}^{+\infty}[\hat{w}(s_{0j}+\upsilon\tau)\chi(s_{0j}+\upsilon\tau)]\,\mathrm{e}^{-\mathrm{i}\omega\tau}\,\mathrm{d}\tau\\ &= \frac{1}{\sqrt{2\pi}}\sum_{j=1}^{J}\Delta_j\int_{-T_{j1}}^{+T_{j2}}\hat{w}(s_{0j}+\upsilon\tau)\,\mathrm{e}^{-\mathrm{i}\omega\tau}\,\mathrm{d}\tau \qquad (45)\\ &= \frac{1}{\sqrt{2\pi}\upsilon}\sum_{j=1}^{J}\Delta_j\int_{0}^{\eta}\mathrm{e}^{-\frac{\mathrm{i}(x-s_{0j})\omega}{\upsilon}}\hat{w}(x)\,\mathrm{d}x, \qquad (46)\end{aligned}$$

where the change of variables ($x \to s_{0j}+\upsilon\tau$, $\mathrm{d}x \to \upsilon\,\mathrm{d}\tau$,) has been made to evaluate the integral. Since $w \equiv \hat{w}$ inside the interval $[0,\eta]$, a comparison of Eqs. (42) and (46) completes the proof. □

References

[1] L. Frýba, *Vibration of Solids and Structures Under Moving Loads*, Telford, London, 1999.
[2] V.V. Krylov, Effects of track properties on ground vibrations generated by high-speed trains, *Acustica* 84-1 (1998) 78–90.
[3] B.Y. Chung, J.L. Jong, W.L. Jong, H.Y. Jin, Y.J. Hee, Ambient vibration tests for structural integrity assessment of bridges, *Proceedings IABMAS'02*, Barcellona, Spain, 2002.
[4] P. Paultre, J. Proulx, M. Talbot, Dynamic testing procedures for highway bridges using traffic loads, *Journal of Structural Engineering ASCE* 121-2 (1995) 362–376.
[5] Y.H. Chen, Y.H. Huang, Dynamic characteristics of infinite and finite railways to moving loads, *Journal of Structural Engineering ASCE* 129-9 (2003) 987–993.
[6] L. Cveticanin, T. Atanackovic, Vibrations of a finite length beam with an axially movable load, *European Journal of Mechanics A/Solids* 15-4 (1996) 667–680.
[7] M.A. Foda, Z. Abduljabbar, A dynamic green function formulation for the response of a beam structure to a moving mass, *Journal of Sound and Vibration* 210-3 (1998) 295–306.
[8] B. Peeters, C.E. Ventura, Comparative study of modal analysis techniques for bridge dynamic characteristics, *Mechanical Systems & Signal Processing* 17-5 (2003) 965–988.
[9] J.C. Araiza, J.R. Casas, Safety assessment of bridges through dynamical tests: state of the art review, *Proceedings IABMAS'02*, Barcellona, Spain, 2002.
[10] J.J. Kalker, Discretely supported rails subjected to transient loads, *Vehicle System Dynamics* 25-1 (1996) 71–88.
[11] V.V. Krylov, Spectra of low-frequency ground vibrations generated by high-speed trains on layered ground, *Journal of Low Frequency Noise Vibration and Active Control* 16-4 (1997) 257–270.
[12] Y.B. Yang, J.D. Yau, L.C. Hsu, Vibration of simple beams due to trains moving at high speeds, *Engineering Structures* 19-11 (1997) 936–944.
[13] D. Liberatore, F. Braga, Dynamic interaction train–railway–structure: the IDTBS code, *Ingegneria Ferroviaria* 12 (1992) 695–700 (in Italian).
[14] B. Biondi, G. Muscolino, A. Sofi, A substructure approach for the dynamic analysis of train–track–bridge system, *Computers and Structures* 83 (28–30 Special issue) (2005) 2271–2281.
[15] E. Esmailzadeh, N. Jalili, Vehicle–passenger–structure interaction of uniform bridges traversed by moving vehicles, *Journal of Sound and Vibration* 260-4 (2003) 611–635.
[16] T.C. Pan, J. Li, Dynamic vehicle element method for transient response of coupled vehicle–structure systems, *Journal of Structural Engineering ASCE* 128-2 (2002) 214–220.
[17] X.Q. Zhu, S.S. Law, Dynamic load on continuous multi-lane bridge deck from moving vehicles, *Journal of Sound and Vibration* 251-4 (2002) 697–716.
[18] A.V. Pesterev, L.A. Bergman, An improved series expansion of the solution to the moving oscillator problem, *ASME Transactions* 122 (2000) 54–61.